

Optimal replica exchange method combined with Tsallis weight sampling

Jaegil Kim^{a)} and John E. Straub^{b)}*Department of Chemistry, Boston University, Boston, Massachusetts 02215, USA*

(Received 5 February 2009; accepted 8 March 2009; published online 14 April 2009)

A unified framework integrating the generalized ensemble sampling associated with the Tsallis weight [C. Tsallis, *J. Stat. Phys.* **52**, 479 (1988)] and the replica exchange method (REM) has been proposed to accelerate the convergence of the conventional temperature REM (*t*-REM). Using the effective temperature formulation of the Tsallis weight sampling, it is shown that the average acceptance probability for configurational swaps between neighboring replicas in the combination of Tsallis weight sampling and REM (Tsallis-REM) is directly proportional to an overlap integral of the energy distributions of neighboring replicas as in the *t*-REM. Based on this observation, we suggest a robust method to select optimal Tsallis parameters in the conventional parametrization scheme and present new parametrization schemes for the Tsallis-REM, which significantly improves the acceptance of configurational swaps by systematically modulating energy overlaps between neighboring replicas. The distinguished feature of our method is that all relevant parameters in the Tsallis-REM are automatically determined from the equilibrium phase simulation using the *t*-REM. The overall performance of our method is explicitly demonstrated for various simulation conditions for the Lennard-Jones 31 atom clusters, exhibiting a double-funneled energy landscape. © 2009 American Institute of Physics. [DOI: 10.1063/1.3108523]

I. INTRODUCTION

The replica exchange method (REM) or parallel tempering (PT)^{1,2} has become a standard tool nowadays to investigate equilibrium properties of diverse complex systems such as biomolecules,^{3–6} supercooled liquids,^{7–9} and atomic clusters,^{10–12} in which conventional canonical ensemble sampling suffers from broken ergodicity due to a rugged energy landscape.¹³ A key element of the REM is to run multiple Markov chains in parallel and swap configurations between neighboring replicas subject to detailed balance.^{14,15} In the standard temperature REM (*t*-REM), each replica samples a canonical ensemble with the Gibbs–Boltzmann weight at a desired temperature. A broken ergodicity of low temperature replicas is significantly diminished and the convergence of simulations is greatly accelerated via configurational exchanges between low and high temperature replicas, which can easily access the relevant configurational space without trapping.

In the conventional *t*-REM, the acceptance of configurational swaps between adjacent replicas is determined by an overlap of energy distributions of nearby replicas. However, as the system size expands, energy overlaps between neighboring replicas rapidly diminish. To maintain a nonvanishing acceptance probability, the average energy separation $\Delta U = C_v(T)\Delta T$, with C_v and ΔT as the heat capacity and the temperature separation of neighboring replicas, respectively, must be comparable to the energy fluctuation $\delta U = T\sqrt{C_v}$ of each replica, i.e., $\Delta U/\delta U = (\Delta T/T)\sqrt{C_v} \sim 1$. Since C_v increases in proportion to f , with f as the number of degrees of freedom, ΔT must decrease in proportion to $1/\sqrt{f}$.¹⁶ To keep

an appreciable acceptance probability, it is necessary to increase the number of replicas in an intermediate temperature region. The growth as \sqrt{f} of the number of replicas requires more configurational swaps to sample the relevant temperature space and leads to a considerable slowing down in the convergence of simulation averages.

During the past decade, several sophisticated REM variants have been developed to resolve the system size dependence of the *t*-REM.^{17–28} One effective way to circumvent a scalability problem of the *t*-REM is to exploit the generalized ensemble method (GEM)^{29–32} in each replica. The use of non-Boltzmann sampling weights of the GEM, yielding a delocalized energy distribution compared to a localized Gaussian of the canonical ensemble, can maintain energy overlaps with fewer replicas and accelerate the convergence of simulation averages via enhanced configurational swaps for an expanded dynamic sampling range. In previous studies,^{33–36} multicanonical sampling (MUCA) has been employed to combine the GEM and the REM, but a prior weight determination in MUCA, which is often nontrivial and requires a long iterative process as the system size increases, limited its practical applicability.

An alternative means of avoiding prior weight determination is to use sampling weights known *a priori*. In this sense, the Tsallis weight originally proposed in nonextensive statistical mechanics³⁷ is an effective workhorse for the combination of the GEM and the REM since the Tsallis weight is fully characterized by a few adjustable parameters and allows a delocalized energy distribution with a proper choice of parameters. Inspired by its initial application for the simulation of atomic clusters,^{38,39} the Tsallis weight sampling has been applied to a variety of complex systems including protein folding,^{31,40–42} molecular docking,⁴³ and atomic

^{a)}Electronic mail: jaegil@bu.edu.^{b)}Electronic mail: straub@bu.edu.

clusters.¹⁰ Inventive use of the Tsallis weight has been further extended to incorporate the REM in the form of the generalized PT (GPT) (Ref. 17) or q -REM.¹⁸

The basic idea of the combination of the Tsallis weight sampling and the REM (Tsallis-REM) is to accelerate the configurational sampling of the original potential energy surface by coupling it to the configurational sampling of the modified potential energy surfaces associated with the parametrized Tsallis weights, which are designed to reduce potential barriers and avoid trapping. However, the main challenge in realizing the potential of this hybrid method is that the overall performance shows a very subtle dependence on the parameter selection intrinsic to the Tsallis weight. The absence of a systematic approach in choosing the optimal Tsallis parameter has limited the use of this novel sampling method. A few attempts have been made to determine optimal Tsallis parameters in a single Tsallis weight sampling by relying on the harmonic approximation for the density of states³¹ or the effective temperature formulation of the Tsallis weight sampling.⁴⁴ However, the validity of these methods has not been rigorously examined in connection with the REM and the detailed study on the optimal selection of the Tsallis parameters in the Tsallis-REM has not been fully addressed.

In the present paper, we present a unified theoretical framework integrating the generalized ensemble sampling associated with the Tsallis weight and the REM via the effective temperature formulation of the Tsallis weight sampling. A key finding is that the average acceptance probability for configurational swaps in the Tsallis-REM is solely determined by an overlap integral of the energy distributions of neighboring replicas due to the linear potential energy dependence of the Tsallis effective temperature. This finding leads to the development of a robust method to determine optimal Tsallis parameters in the conventional parametrization scheme of the Tsallis-REM. The acceptance of configurational swaps is significantly improved through the systematic modulation of energy overlaps between neighboring replicas.

Using the one-to-one correspondence between the Tsallis weight and its effective temperature, we also present new parametrization schemes for the Tsallis-REM in which all relevant Tsallis parameters are optimally chosen from the equilibrium phase simulation in the t -REM to maximize the acceptance of configurational swaps. We demonstrate the superior performance of our algorithm relative to the conventional t -REM by analyzing thermodynamic properties and tunneling events in replica and energy space in Lennard-Jones (LJ) 31 atomic clusters, exhibiting a double-funneled energy landscape.

In Sec. II, a theoretical formulation of the Tsallis-REM is presented with an optimal performance condition, maximizing the acceptance of replica exchanges. In Sec. III, applying the effective temperature formulation of the Tsallis weight sampling, a novel method to determine optimal Tsallis parameters is suggested in three different parametrization schemes. In Sec. IV, the global convergence of the Tsallis-REM has been examined and quantitatively compared to that

of the standard t -REM in applications to the 31 atom LJ cluster in various simulation conditions. A conclusion and brief summary are presented in Sec. V.

II. TSALLIS-REM

A. Configurational sampling in each replica

Let us start by considering the most general form of the Tsallis weight^{38,39} for a given configuration \mathbf{x} as

$$\mathcal{W}_\alpha(\mathbf{x}) = [\beta_\alpha^{-1} - (1 - q_\alpha)(U(\mathbf{x}) - U_\alpha)]^{1/(1-q_\alpha)}, \quad (1)$$

where $U(\mathbf{x})$ is the original potential energy function, β_α is the inverse temperature $[k_B T_\alpha]^{-1}$ ($k_B=1$), q_α is the Tsallis entropy index, and U_α is the reference energy to guarantee $\mathcal{W}_\alpha > 0$. The subscript α represents the replica index. Notice that $\mathcal{W}_\alpha(\mathbf{x})$ reduces to the Gibbs–Boltzmann weight $\mathcal{W}_{\text{GB}}(\mathbf{x}) \sim \exp\{-\beta_\alpha(U - U_\alpha)\}$ in the limit of $q_\alpha \rightarrow 1$. In the usual implementation of the Tsallis-REM (GPT or q -REM), the reference replica samples the original potential energy surface with $q_\alpha=1$ at the fixed β_α and U_α , and other replicas sample the deformed potential energy surfaces associated with the Tsallis weights with $q_{\alpha'} > 1$ ($\alpha' \neq \alpha$). The coupling or configurational mixing between the reference replica and other replicas via the configurational swaps offers an “escaping route” for the reference replica from trapped states and enables an accelerated configurational sampling.

In the Tsallis-REM, a trial move from \mathbf{x} to \mathbf{x}' in α th replica is accepted by the standard Metropolis criterion

$$A_{\text{intra}}(\mathbf{x} \rightarrow \mathbf{x}') = \min[1, \exp\{w_\alpha(\mathbf{x}) - w_\alpha(\mathbf{x}')\}], \quad (2)$$

where $w_\alpha(\mathbf{x})$ is the Tsallis effective potential defined as

$$\begin{aligned} w_\alpha(\mathbf{x}) &= -\ln \mathcal{W}_\alpha(\mathbf{x}) \\ &= \frac{1}{(q_\alpha - 1)} \ln[\beta_\alpha^{-1} + (q_\alpha - 1)(U(\mathbf{x}) - U_\alpha)]. \end{aligned} \quad (3)$$

The mathematical transformation [Eq. (3)] with a proper choice of Tsallis parameters facilitates a configurational sampling by smoothing the original potential energy surface.³⁹ The underlying mechanism of potential smoothing is apparent in the approximate acceptance probability $\tilde{A}_{\text{intra}}(\mathbf{x} \rightarrow \mathbf{x}')$ of Eq. (2) as

$$\tilde{A}_{\text{intra}}(\mathbf{x} \rightarrow \mathbf{x}') \approx \min[1, \exp\{-\tilde{\beta}_\alpha(U)(U' - U)\}], \quad (4)$$

where $U' = U(\mathbf{x}')$ and $\tilde{\beta}_\alpha(U) = [\partial w_\alpha / \partial U]^{-1}$ is the inverse Tsallis effective temperature. In Eq. (4) we used the linear expansion of $w_\alpha(U') = w_\alpha(U) + \tilde{\beta}_\alpha(U)(U' - U)$ by assuming that $|U' - U| \ll 1$, which obeys in most local trial moves. Notice that the inverse Tsallis effective temperature $\tilde{\beta}_\alpha(U)$ reduces to the physical inverse temperature β_α in the Gibbs–Boltzmann limit with $q_\alpha \rightarrow 1$. Based on the asymptotic correspondence between $\tilde{\beta}_\alpha(U)$ and β_α , we define the Tsallis effective temperature $\tilde{T}_\alpha(U) = [\tilde{\beta}_\alpha(U)]^{-1}$ as

$$\tilde{T}_\alpha(U) = T_\alpha + (q_\alpha - 1)(U - U_\alpha) \quad (5)$$

so that the approximate acceptance in the Tsallis weight sampling is simply

$$\tilde{A}_{\text{intra}}(\mathbf{x} \rightarrow \mathbf{x}') \approx \min[1, \exp\{-\gamma_{\alpha}(U)\beta_{\alpha}(U' - U)\}], \quad (6)$$

where $\gamma_{\alpha}(U) = T_{\alpha}/\tilde{T}_{\alpha}(U)$ is the energy-dependent scaling factor.

Equation (6) reveals that the Tsallis weight sampling on the deformed potential energy surface $w_{\alpha}(\mathbf{x})$ is equivalent to a Metropolis sampling combined with the energy-dependent temperature $\tilde{T}_{\alpha}(U)$ on the original potential energy surface $U(\mathbf{x})$. Of particular importance is that $\gamma_{\alpha}(U)$ can be made to be less than unity throughout the configurational space with the choice of $q_{\alpha} > 1$ and $U_{\alpha} = U_{\text{min}}$, the global minimum energy. Choosing $q_{\alpha} > 1$ and $U_{\alpha} < U_{\text{min}}$ makes $\tilde{A}_{\text{intra}}(\mathbf{x} \rightarrow \mathbf{x}')$ always greater than the Metropolis acceptance, i.e., $\min[1, \exp\{-\beta_{\alpha}(U' - U)\}]$ in a canonical ensemble for energy-increasing trial moves. This property allows the system to escape from trapped states more easily with a more frequent visit to a higher energy region, while preserving the acceptance of energy-decreasing moves as in the Gibbs–Boltzmann sampling.

The concept of the effective temperature plays a key role in the understanding of the Tsallis weight sampling. It also provides a convenient framework to analyze the sampling dynamics of variants of the GEM such as MUCA^{45,46} and simulated tempering.^{47,48} As will be discussed, many essential properties of the Tsallis weight sampling originate in the linear dependence of the Tsallis effective temperature with respect to the potential energy U in Eq. (5).

B. Configurational swaps between neighboring replicas

A trial configurational swap (or replica exchange) between neighboring Tsallis sampling runs is accepted with probability

$$A_{\text{inter}}(\alpha; \mathbf{x}\mathbf{x}') = \min[1, \exp(\Delta_{\alpha})], \quad (7)$$

where $\Delta_{\alpha} = w_{\alpha+1}(U') - w_{\alpha+1}(U) + w_{\alpha}(U) - w_{\alpha}(U')$. In terms of the Tsallis effective temperature, the exponent in Eq. (7) further transforms to

$$\Delta_{\alpha}(U, U') = \int_U^{U'} [\tilde{\beta}_{\alpha+1}(z) - \tilde{\beta}_{\alpha}(z)] dz. \quad (8)$$

The overall performance of the REM is intimately connected to the success rate of replica exchanges. This rate is often quantified by the average acceptance probability $p_{\text{acc}}(\alpha) = N_{\text{accept}}/N_{\text{trial}}$, with N_{accept} and N_{trial} as the number of accepted and attempted replica exchanges of the α th replica. Assuming that the normalized probability density function (PDF) of the Tsallis weight sampling is known, $p_{\text{acc}}(\alpha)$ is determined as

$$p_{\text{acc}}(\alpha) = \int dU dU' J(U, U') \min[1, \exp(\Delta_{\alpha})], \quad (9)$$

where $J(U, U') = P_{\alpha}(U)P_{\alpha+1}(U')$ is the joint probability that neighboring replicas have the energies U and U' . Applying the formal relationship $P_{\alpha}(U) = \Omega(U)\mathcal{W}_{\alpha}(U)$, with $\Omega(U)$ as the density of states, and algebraic operations yield

$$p_{\text{acc}}(\alpha) = \int dU dU' \theta(\Delta_{\alpha}) P_{\alpha}(U) P_{\alpha+1}(U') + \int dU dU' \theta(-\Delta_{\alpha}) P_{\alpha}(U') P_{\alpha+1}(U), \quad (10)$$

where $\theta(z)$ is the Heaviside step function defined as one for $z > 0$ and zero for otherwise. Denoting $\Delta_{\alpha}(U, U') = -\Delta_{\alpha}(U', U)$ in Eq. (8) yields

$$p_{\text{acc}}(\alpha) = 2 \int dU dU' P_{\alpha}(U) P_{\alpha+1}(U') \theta(\Delta_{\alpha}). \quad (11)$$

In the Gibbs–Boltzmann limit $q_{\alpha} \rightarrow 1$, $\theta(\Delta_{\alpha}) = \theta(U - U')$ since $\tilde{\beta}_{\alpha+1}(U) = \beta_{\alpha+1} < \tilde{\beta}_{\alpha}(U) = \beta_{\alpha}$, and Eq. (11) becomes an overlap integral of canonical PDFs^{49,50} as

$$p_{\text{acc}}^{\text{GB}}(\alpha) = 2 \int_{-\infty}^{\infty} dU P_{\alpha}(U) \int_{-\infty}^U dU' P_{\alpha+1}(U'). \quad (12)$$

A key observation in Eq. (11) is that $p_{\text{acc}}(\alpha)$ is solely represented in terms of the effective temperatures of neighboring replicas through Eq. (8) and the formal expression

$$P_{\alpha}(U) \sim \exp\left\{ \int^U \left[\frac{1}{T_S(z)} - \frac{1}{\tilde{T}_{\alpha}(z)} \right] dz \right\}, \quad (13)$$

where $T_S(U) = [\partial S / \partial U]^{-1}$ is the statistical temperature,⁵¹ with $S(U) = \ln \Omega(U)$ as the microcanonical entropy. This implies that $p_{\text{acc}}(\alpha)$ in the Tsallis-REM can be systematically improved by adjusting Tsallis parameters in $\tilde{T}_{\alpha}(U)$. Note that all relevant Tsallis parameters are contained in $\tilde{T}_{\alpha}(U)$.

The strategy to determine optimal weight parameters maximizing $p_{\text{acc}}(\alpha)$ is facilitated by using Tsallis weight sampling. The Tsallis effective temperature is a simple linear function of U , which simplifies $\theta(\Delta_{\alpha})$. In the conventional GPT (Ref. 17) or q -REM (Ref. 18) employing the Tsallis entropy index q_{α} as a control parameter at the fixed $T_{\alpha} = T_0$ and $U_{\alpha} = U_0$, one of the q values (for example, $\alpha = 1$) is set to unity to sample the canonical ensemble at the temperature T_0 . A range of q_{α} ($\alpha = 2, \dots, M$) values are assigned in an ascending order ($q_1 = 1 < q_2 < \dots < q_M$) for other replicas, with M as the number of replicas. In this parametrization scheme, $\Delta_{\alpha}(U, U')$ in Eq. (8) simply reduces to $\theta(U - U')$ by identifying that $(q_{\alpha} - 1)$ is the slope of the linear effective temperature since $\tilde{T}_{\alpha+1}(U) \geq \tilde{T}_{\alpha}(U)$ for all U with $U_0 < U_{\text{min}}$. The overlap integral [Eq. (12)] determines $p_{\text{acc}}(\alpha)$ in the Tsallis-REM, exactly as in the t -REM. As a result, the optimal performance condition in the Tsallis-REM maximizing $p_{\text{acc}}(\alpha)$ reduces to choosing proper Tsallis parameters that optimize overlap integrals between neighboring energy distributions, which is achieved through more delocalized Tsallis PDFs.

C. Parameter dependence of a Tsallis PDF

As the optimal $p_{\text{acc}}(\alpha)$ is achieved by maximizing overlap integrals of neighboring Tsallis PDFs, it is essential to understand how each $P_{\alpha}(U)$ varies with changing relevant parameters. The approximate form of $P_{\alpha}(U)$ and its param-

eter dependence can be analyzed by using a local expansion of Eq. (13) in the vicinity of the stationary point U^* satisfying $\partial \ln P_\alpha(U^*)=0$ as

$$\ln P_\alpha(U) \approx \ln P_\alpha(U^*) - \frac{1}{2\sigma_q}(U - U^*)^2 + \dots, \quad (14)$$

where U^* is the crossing point between the statistical temperature and the Tsallis effective temperature, i.e., $\tilde{T}_\alpha(U^*) = T_S(U^*) = T^*$, and σ_q is the Gaussian width of the Tsallis PDF defined as

$$\sigma_q(U^*) = \left[\frac{T'_S(U)}{T_S^2(U)} - \frac{\tilde{T}'_\alpha(U)}{\tilde{T}_\alpha^2(U)} \right]_{U=U^*}^{-1}, \quad (15)$$

where $T'_S(U) = \partial T_S / \partial U$ and $\tilde{T}'_\alpha(U) = \partial \tilde{T}_\alpha / \partial U$. When $T_S(U)$ is well approximated by a linear function around U^* , the equivalence between the canonical and microcanonical ensembles yields $T'_S(U^*) = 1/C_v(T^*)$ and the q_α -dependent Gaussian width further reduces to

$$\sigma_q(U^*) = \sigma_0(1 - \kappa), \quad (16)$$

where $\kappa = (q_\alpha - 1)/T'_S(U^*)$ and $\sigma_0 = T^{*2}/T'_S(U^*)$ is the Gaussian width of the canonical PDF at the temperature T^* . In Eq. (16), $\sigma_q \rightarrow \sigma_0$ in the Gibbs–Boltzmann limit of $q_\alpha \rightarrow 1$.

Equations (14) and (16) expose an interesting dependence of the Tsallis PDF on q_α . For $1 < q_\alpha < 1 + q_c$, $q_c = T'_S(U^*)$, $P_\alpha(U)$ becomes much broader than the canonical PDF at the temperature T^* since $\sigma_q > \sigma_0$, while its distribution becomes narrower for $q_\alpha < 1$. In both cases, the maximum of the Tsallis PDF is centered at the stable crossing point U^* . For the case of $q_\alpha = 1 + q_c$, in which the Tsallis effective temperature is tangential to $T_S(U)$ at U^* , $P_\alpha(U)$ becomes locally flat around U^* , which indicates a case of marginal stability. Choosing $q_\alpha = 1 + q_c$ produces the most delocalized Tsallis PDF in a single Tsallis weight sampling.⁴⁴ As q_α exceeds q_c , the local expansion analysis breaks down and U^* makes an unstable crossing point corresponding to a local minimum of $P_\alpha(U)$.

D. Reweighting

After a long production run with properly chosen Tsallis parameters, the weighted histogram method⁵² is applied to join multiple Tsallis weight samplings and determine the density of states estimate as

$$\tilde{\Omega}(U) = \frac{\sum_{\alpha=1}^M N_\alpha P_\alpha(U)}{\sum_{\alpha=1}^M N_\alpha Z_\alpha^{-1} e^{-w_\alpha(U)}}, \quad (17)$$

where $P_\alpha(U)$ is the Tsallis PDF and N_α is the number of data samples in the α th replica. The relative partition function Z_α is calculated self-consistently using

$$Z_{\alpha'} = \sum_U \frac{\sum_{\alpha=1}^M N_\alpha P_\alpha(U)}{\sum_{\alpha=1}^M N_\alpha Z_\alpha^{-1} e^{-[w_\alpha(U) - w_{\alpha'}(U)]}}. \quad (18)$$

Once the density of states is computed, all canonical thermodynamic properties can be calculated at an arbitrary temperature.

III. EFFECTIVE TEMPERATURE SCHEMES TO DETERMINE OPTIMAL TSALLIS PARAMETERS

Based on the key finding that the Tsallis PDF of each replica is a delocalized Gaussian, centered at the stable crossing point U^* between $T_S(U)$ and $\tilde{T}_\alpha(U)$ for $1 \leq \tilde{q}_\alpha = q_\alpha - 1 < q_c$, the overlap integral in Eq. (11) can be systematically improved by modulating relevant Tsallis parameters to ensure that $\tilde{T}_\alpha(U)$ forms stable crossing points with $T_S(U)$ in (U, T) space. Notice that the Tsallis PDF becomes more and more delocalized as \tilde{q}_α approaches $q_c = T'_S(U^*)$. Exploiting the fact that $\tilde{T}_\alpha(U)$ is a linear function of U , several parametrization schemes can be designed to maximize energy overlaps of the Tsallis PDFs.

A. Parametrization scheme I in GPT or q -REM

In the conventional GPT or q -REM, the Tsallis entropy index q_α is a control parameter characterizing the sampling weight in each replica with fixed $T_\alpha = T_0$ and $U_\alpha = U_0$. In this case, all Tsallis effective temperatures cross the common fixed point (U_0, T_0) , as shown in Fig. 1(a), regardless of the value of \tilde{q}_α with

$$\tilde{T}_\alpha^I(U) = T_0 + \tilde{q}_\alpha(U - U_0), \quad (19)$$

where the superscript I in $\tilde{T}_\alpha^I(U)$ denotes the first parametrization scheme. In scheme I, the location of (U_0, T_0) plays an important role in determining the parameter range of \tilde{q}_α and should be carefully chosen to make $\tilde{T}_\alpha(U)$ form stable crossing points with $T_S(U)$. To determine an optimal \tilde{q}_α , the approximate form of $T_S(U)$ should be guessed before the simulation. We applied the linear approximation for $T_S(U)$ (Refs. 45 and 46) as

$$\tilde{T}_S(U) \approx \tilde{q}_{LH}(U - U_L) + T_L, \quad (20)$$

where $\tilde{q}_{LH} = (T_H - T_L) / (\tilde{U}_H - \tilde{U}_L)$ is the slope connecting two thermodynamic points of (\tilde{U}_L, T_L) and (\tilde{U}_H, T_H) , with \tilde{U}_L and \tilde{U}_H as the approximate average energies at the lowest and highest temperatures of T_L and T_H , respectively. The linear approximation in Eq. (20) is fairly effective except for the phase transition regions associated with the van der Waals loop or S -loop^{53,54} in the statistical temperature.

The process followed in selecting the optimal \tilde{q}_α in the conventional GPT or q -REM consists of three steps.

- (i) Identify the temperature range of interest $[T_L, T_H]$ and allocate the sampling temperatures t_α between T_L and T_H . The intermediate temperatures t_α ($\alpha=2, \dots, M-1$) are sequentially distributed in ascending order

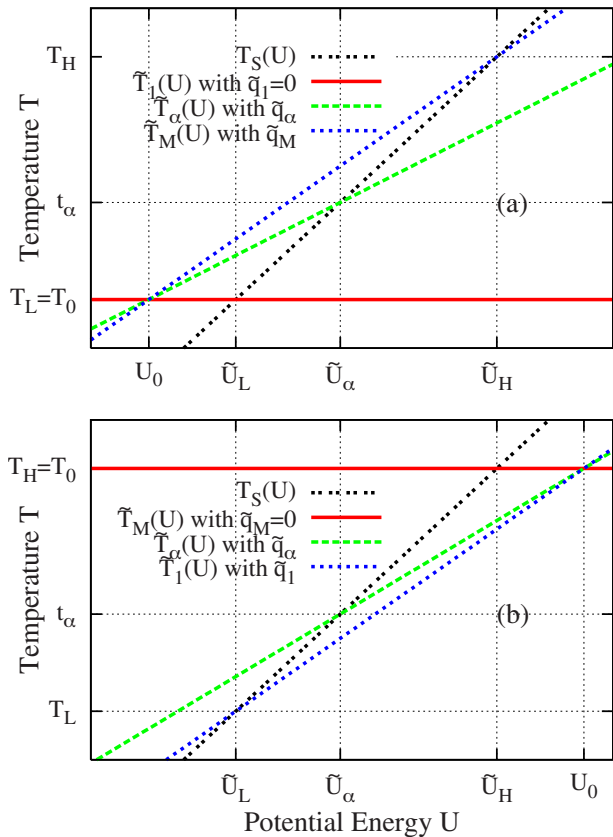


FIG. 1. (Color online) Statistical temperature $T_S(U)$ and Tsallis effective temperatures $\tilde{T}_\alpha(U)$ in (a) parametrization scheme I with ($U_0 < \tilde{U}_L, T_0 = T_L$) and (b) ($U_0 > \tilde{U}_H, T_0 = T_H$). Here $T_S(U)$ is assumed to be a linear function of U . The intermediate points of $(\tilde{U}_\alpha, t_\alpha)$ ($1 < \alpha < M$) are determined from the equilibrium phase in the conventional t -REM.

employing the geometric or equidistant temperature scheme as $t_\alpha = T_L(T_H/T_L)^{(\alpha-1)/(M-1)}$ and $t_\alpha = T_L + (\alpha - 1)(T_H - T_L)/(M - 1)$, respectively.

- (ii) Locate the common fixed point (U_0, T_0) at an appropriate region in (U, T) space to form stable crossing points between $\tilde{T}_\alpha(U)$ and $\tilde{T}_S(U)$. One reasonable option is $T_0 = T_L$ with $U_0 < \tilde{U}_L$, as depicted in Fig. 1(a). In this case, the lowest replica samples the original potential energy surface with $\tilde{q}_1 = 0$ at T_L and other replicas sample higher energy regions on the deformed potential surfaces with $\tilde{q}_\alpha > 0$ ($\alpha = 2, \dots, M$). The parameter \tilde{q}_α ranges from zero to \tilde{q}_M , $\tilde{q}_M = (T_H - T_0)/(\tilde{U}_H - U_0)$. The other option is $T_0 = T_H$ with $U_0 > \tilde{U}_H$, as depicted in Fig. 1(b), in which the highest replica samples the original potential energy surface with $\tilde{q}_M = 0$ at T_H and other replicas sample lower energy regions with $\tilde{q}_\alpha > 0$ ($\alpha = 1, \dots, M - 1$). The parameter \tilde{q}_α ranges from q_1 to zero, $\tilde{q}_1 = (T_L - T_0)/(\tilde{U}_L - U_0)$. The first option for (U_0, T_0) is useful when the canonical ensemble sampling at the temperature T_L is of interest. The second option is suitable for extensive sampling of low energy regions since the increased \tilde{q}_α creates a more delocalized Tsallis PDF at lower energy regions.
- (iii) The choice of intermediate \tilde{q}_α values between \tilde{q}_1 and

\tilde{q}_M is crucial for the optimal performance of the Tsallis-REM. The intermediate values of \tilde{q}_α ($2 < \alpha < M - 1$) are automatically determined to make each $\tilde{T}_\alpha(U)$ cross $T_S(U)$ at the approximate average energy $(\tilde{U}_\alpha, t_\alpha)$, determined by taking an average of the canonical ensemble data at each t_α in the equilibrium phase of a t -REM simulation as

$$\tilde{q}_\alpha = (t_\alpha - T_0)/(\tilde{U}_\alpha - U_0). \quad (21)$$

Note that once the common fixed point (U_0, T_0) is determined, all relevant Tsallis parameters \tilde{q}_α are automatically determined from the equilibrium phase t -REM with the input parameters (\tilde{U}_L, T_L) and (\tilde{U}_H, T_H) , which can be computed using short canonical runs at T_L and T_H , respectively.

B. Parametrization scheme II

The one-to-one mapping between the effective temperature and the sampling weight

$$\mathcal{W}_\alpha(\mathbf{x}; \xi) \sim \exp \left\{ - \int^U \tilde{T}_\alpha^{-1}(z; \xi) dz \right\} \quad (22)$$

allows for new parametrization schemes in the Tsallis-REM. Once the effective temperature is properly defined as a function of U with a set of parameters (ξ_1, ξ_2, \dots) , the generalized sampling weight is uniquely determined.

The second parametrization scheme utilizes T_α in Eq. (1) as a control parameter with fixed $\tilde{q}_\alpha = q_0$ and $U_\alpha = 0$ (as opposed to \tilde{q}_α in scheme I). As seen in Fig. 2(a), the Tsallis effective temperatures are parallel to each other in (U, T) space with different T -intercepts and the same slopes $\tilde{q}_0 = q_0 - 1$ since

$$\tilde{T}_\alpha^{\text{II}}(U) = T_\alpha + \tilde{q}_0 U. \quad (23)$$

The slope \tilde{q}_0 should be properly chosen to make $\tilde{T}_\alpha(U)$ form stable crossing points with $\tilde{T}_S(U)$ at $(\tilde{U}_\alpha, t_\alpha)$. Once \tilde{q}_0 is determined, the control parameter T_α is identified as $t_\alpha - \tilde{q}_0 \tilde{U}_\alpha$. One criterion for \tilde{q}_0 is that it should be smaller than the slope $\tilde{q}_{LH} = (T_H - T_L)/(\tilde{U}_H - \tilde{U}_L)$ connecting (\tilde{U}_L, T_L) and (\tilde{U}_H, T_H) because $\tilde{q}_0 > \tilde{q}_{LH}$ may create unstable crossing points at intermediate $(\tilde{U}_\alpha, t_\alpha)$. This scheme is most effective when $T_S(U)$ is well approximated by a linear function, in which the Tsallis PDFs are nearly identical Gaussians with the width $\sigma_q = \sigma_0/(1 - \tilde{q}_0/\tilde{q}_{LH})$ regardless of α .

C. Parametrization scheme III

In contrast to parametrization schemes I and II, which employ a single parameter q_α or T_α for characterizing the sampling weight, respectively, a set of parameters $(\tilde{q}_\alpha, U_\alpha, T_\alpha)$ can be utilized to ensure that each $\tilde{T}_\alpha(U)$ forms a stable crossing point with $T_S(U)$ at $(\tilde{U}_\alpha, t_\alpha)$ as

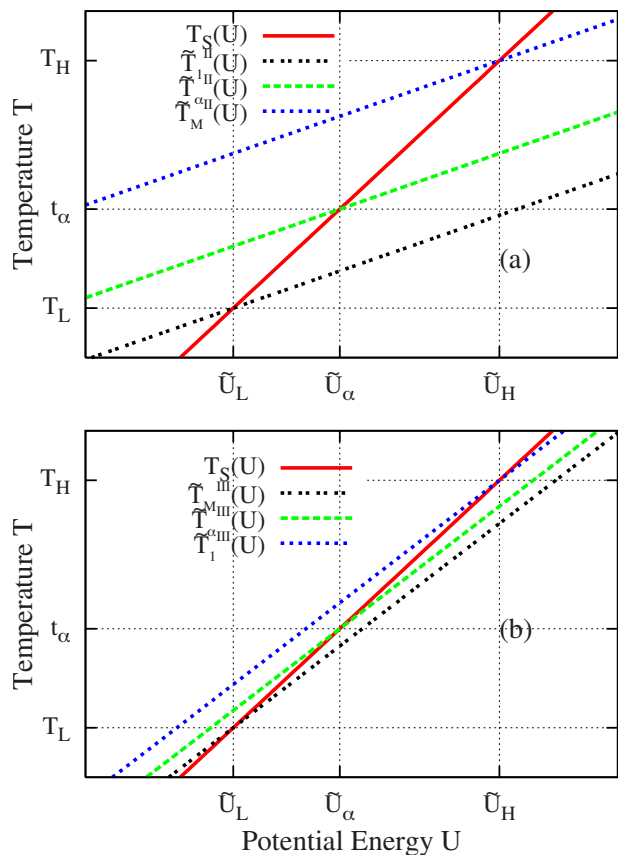


FIG. 2. (Color online) Statistical temperature $T_S(U)$ and Tsallis effective temperatures $\tilde{T}_\alpha(U)$ in (a) parametrization scheme II with the constant slope \tilde{q}_0 and different T_α , and (b) scheme III with a set of multiple parameters $(\tilde{q}_\alpha, U_\alpha, T_\alpha)$. For a linear $T_S(U)$ both schemes II and III become equivalent when setting $\tilde{q}_0 = \gamma \tilde{q}_{LH}$. However, in a curved $T_S(U)$, scheme III is more effective than scheme II.

$$T_\alpha^{\text{III}}(U) = t_\alpha + \tilde{q}_\alpha(U - \tilde{U}_\alpha), \quad (24)$$

where the replica-dependent slope \tilde{q}_α is chosen as $\gamma \tilde{q}_\alpha^{\text{min}}$, with $\tilde{q}_\alpha^{\text{min}}$ as the minimum value of all possible slopes connecting $(\tilde{U}_\alpha, t_\alpha)$ and $(\tilde{U}_{\alpha'}, t_{\alpha'})$ ($\alpha' \neq \alpha$) i.e., $\min\{\tilde{q}_{\alpha\alpha'}\}$, $\tilde{q}_{\alpha\alpha'} = (t_{\alpha'} - t_\alpha) / (\tilde{U}_{\alpha'} - \tilde{U}_\alpha)$. Here we have introduced the extra scaling factor γ ($0 \leq \gamma \leq 1$) to scale down $\tilde{q}_\alpha^{\text{min}}$ so that $\tilde{T}_\alpha(U)$ forms a unique stable crossing point with $T_S(U)$ at $(\tilde{U}_\alpha, t_\alpha)$. Typically, γ is chosen to be less than unity to address a possible uncertainty in $\tilde{U}_\alpha(t_\alpha)$ caused by a too short equilibrium time in the preceding t -REM simulation.

In comparison to scheme II, the adjustable slope \tilde{q}_α allows a fine tuning for $\tilde{T}_\alpha(U)$ so that each effective temperature can be made to be more tangential to $T_S(U)$ at $(\tilde{U}_\alpha, t_\alpha)$, as seen in Fig. 2(b). With prefixed γ , all Tsallis parameters are determined in an automatic fashion from the equilibrium phase of the t -REM simulation without prior knowledge on $T_S(U)$. This scheme is effective for both linear and curved $T_S(U)$. When $T_S(U)$ is a linear function of U , scheme III becomes equivalent to scheme II by setting $\tilde{q}_0 = \gamma \tilde{q}_{LH}$ since $\tilde{q}_\alpha^{\text{min}} \approx \tilde{q}_{LH}$.

IV. APPLICATIONS: LJ 31 ATOM CLUSTERS

The performance of our proposed method has been examined for the case of LJ clusters with $N=31$ (LJ₃₁). LJ

atomic clusters have long been used as benchmark systems in the evaluation of several enhanced sampling algorithms.^{10,12,23,38,44,48} The potential energy of N -atom LJ clusters is given by $E = 4\epsilon \sum_{i < j}^N [(\sigma/r_{ij})^{12} - (\sigma/r_{ij})^6]$, with ϵ and σ as units of energy and length, respectively.

Due to the double-funneled energy landscape of LJ₃₁, associated with the Mackay \rightarrow anti-Mackay transition, the heat capacity displays a narrow peak around $T \approx 0.027$ besides a core melting peak around $T \approx 0.32$. This solid-solid transition is very sensitive to the convergence of simulations,^{11,12,23,55} which makes LJ₃₁ a good benchmark for newly developed sampling algorithms in a rugged energy landscape. A recent study¹² reported that a single replica enhanced sampling employing the Wang–Landau⁵⁶ or the multicanonical algorithm²⁹ failed to capture a correct thermodynamics of the solid-solid transition. The reference thermodynamic data for LJ₃₁ have been determined by the conventional t -REM using 35 replicas for 10^{10} Monte Carlo (MC) cycles in the temperature range of $0.01 \leq T \leq 0.4$. In both t -REM and Tsallis-REM simulations, the geometric temperature allocation was applied with a reflecting wall imposed at the radius of $R_c = 2.5\sigma$. Replica exchange was attempted every 35 MC cycles.

A. Parametrization scheme I

We first performed short canonical runs for 10^6 MC cycles at $T_L = 0.01$ and $T_H = 0.4$. That data provided an estimate of $\tilde{T}_S(U)$ as a linear function connecting $(\tilde{U}_L, T_L) = (0.01, -133.15)$ and $(\tilde{U}_H, T_H) = (0.4, -102.12)$. Based on the estimated $\tilde{T}_S(U)$, four independent Tsallis-REM simulations were performed with four different fixed points (U_0, T_0) taken to be $(-200, 0.0098)$, $(-90, 0.401)$, $(-200, -0.35)$, and $(-80, 0.52)$, as described in Sec. III A.

Through equilibrium phase t -REM simulations, intermediate crossing points $(\tilde{U}_\alpha, t_\alpha)$ are determined by averaging the canonical simulation data at each temperature t_α for 10^6 MC cycles per replica. Once the slope \tilde{q}_α in $\tilde{T}_\alpha(U)$ is determined using Eq. (21), the t -REM was switched to the Tsallis-REM.

As seen in Tsallis-REM employing $(U_0, T_0) = (-200, 0.0098)$ in Fig. 3(a), the crossing points $(\tilde{U}_\alpha, t_\alpha)$ between $\tilde{T}_\alpha(U)$ and $T_S(U) = \tilde{U}^{-1}(U)$ exactly correspond to the maxima of the Tsallis PDFs $P_\alpha(U)$ in Fig. 3(b). The average energy $\bar{U}(T)$ was calculated from the t -REM for 10^{10} MC cycles. The comparison of Tsallis PDFs (line points) with the reweighted canonical PDFs (lines) at t_α in Fig. 3(b) reveals that lower replicas ($\alpha \leq 20$) sample essentially the same energy range as the canonical ensemble with $\tilde{q}_\alpha \approx 0$, while higher replicas ($\alpha > 20$) sample more delocalized energy distributions as \tilde{q}_α increases from zero. The enhancement of energy overlaps is more dramatic in the Tsallis-REM with $(U_0, T_0) = (-80, 0.52)$ in Fig. 4(a). The Tsallis PDFs (line points) are much broader than the reweighted canonical PDFs (lines) for even low temperature replicas and display a

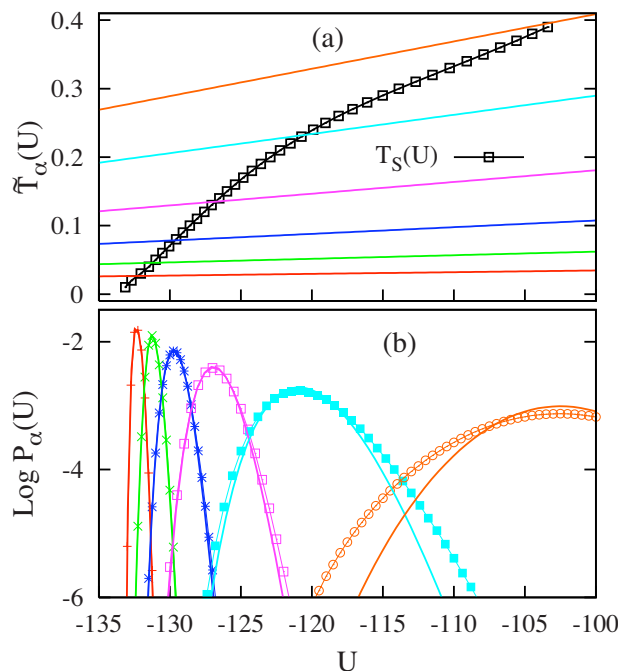


FIG. 3. (Color online) (a) Statistical temperature $T_S(U)$ and Tsallis effective temperatures $\tilde{T}_\alpha(U)$ with $(U_0, T_0) = (-200, 0.0098)$, and (b) Tsallis PDFs (line points) and the reweighted canonical PDFs (solid lines). From bottom to top $\alpha = 10, 15, 20, 25, 30$, and 35 at $U = -135$ in (a).

long tail in the high energy region ($\alpha = 30$) in Fig. 4(b), in which the linear effective temperature $\tilde{T}_{30}(U)$ provides a good approximation to $\tilde{T}_S(U)$ in Fig. 4(a).

The increased energy overlaps due to the delocalized energy distributions in the Tsallis-REM lead to the acceleration of replica exchanges, as seen in Fig. 5(a). The accep-

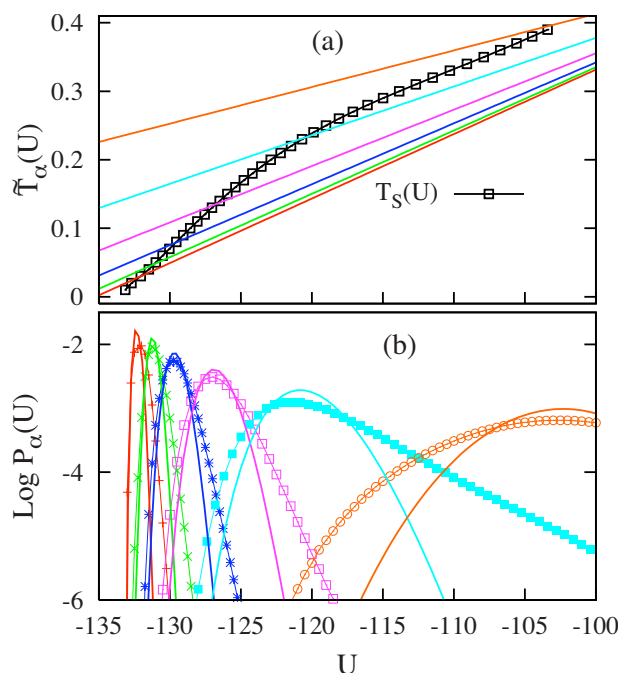


FIG. 4. (Color online) (a) Statistical temperature $T_S(U)$ and Tsallis effective temperatures $\tilde{T}_\alpha(U)$ with $(U_0, T_0) = (-80, 0.52)$, and (b) Tsallis PDFs (line points) and reweighted canonical PDFs (solid lines). From bottom to top $\alpha = 10, 15, 20, 25, 30$, and 35 at $U = -135$ in (a).

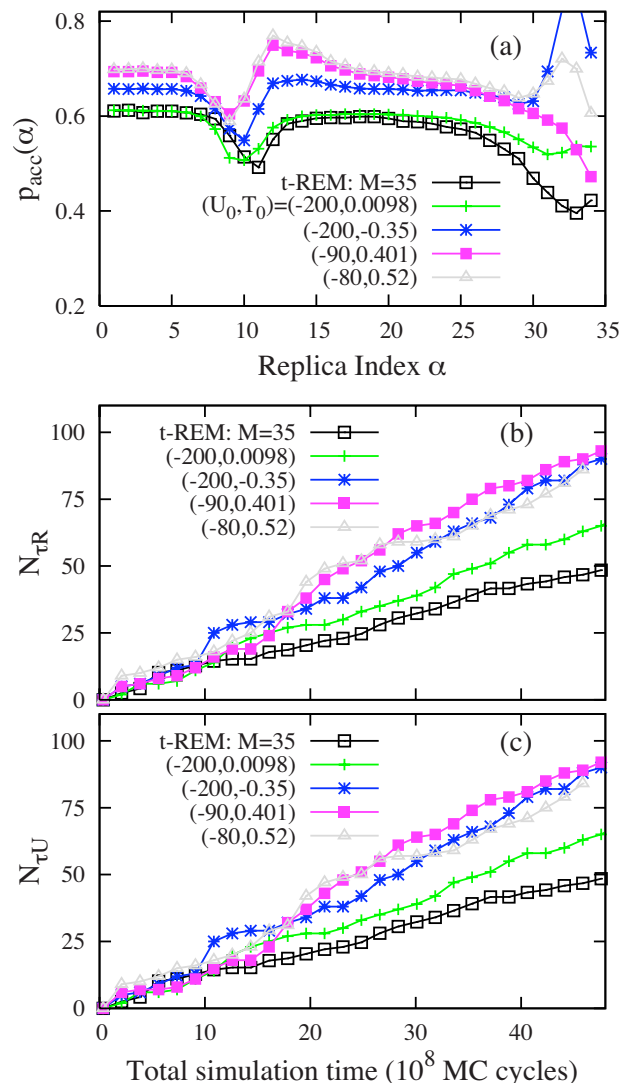


FIG. 5. (Color online) (a) $p_{\text{acc}}(\alpha)$ as a function of the replica index α and accumulated tunneling events in (b) replica space and (c) energy space with varying (U_0, T_0) in parametrization scheme I. $N_{\tau U}$ has been counted for the bounded energy region $[-133, -105]$.

tance probability of the Tsallis-REM is always higher than that of the t -REM for all replicas irrespective of (U_0, T_0) . As predicted by the “incomplete beta-function law,”^{49,50} $p_{\text{acc}}(\alpha)$ in the t -REM in Fig. 5(a) is almost uniform for temperatures where the heat capacity is slowly varying [see Fig. 10(a)]. However, $p_{\text{acc}}(\alpha)$ drops rapidly in the solid-solid ($\alpha = 11$) and the solid-liquid ($\alpha = 33$) transition regions. A similar trend is observed in the Tsallis-REM with a minimum dip around the solid-solid transition region. However, the overall enhancement is apparent for all replicas and most dramatically demonstrated for $(U_0, T_0) = (-80, 0.52)$ and $(90, 0.401)$. In all Tsallis-REM simulations, $p_{\text{acc}}(\alpha)$ approaches that of the t -REM as $\tilde{q}_\alpha \rightarrow 0$ as found in low temperature replicas of $(\tilde{U}_0, T_0) = (-200, 0.0098)$ and high temperature replicas of $(\tilde{U}_0, T_0) = (-90, 0.401)$.

The convergence of simulations of LJ₃₁ is very slow,^{12,23,55} which makes it difficult to evaluate the performance in terms of thermodynamic observables. We carried out a systematic evaluation of performance by counting tun-

neling events in both replica and energy spaces.^{12,29,57} The accumulated tunneling events in replica and energy spaces, $N_{\tau R}$ and $N_{\tau U}$, respectively, quantify how often all replicas sweep the temperature and energy space, from one end to the other, during the simulation. A tunneling event in temperature space occurs when each replica makes a transition from 1 to M or M to 1, while a tunneling in energy space is counted when a replica travels between the two boundary energies of -133 and -105 . Since the convergence of simulations is directly proportional to a diffusivity in replica and energy spaces, both $N_{\tau R}$ and $N_{\tau U}$ provide an effective measure of global convergence of the simulations.

The tunneling events in the Tsallis-REM are significantly higher than observed for t -REM regardless of (U_0, T_0) , as depicted in both Figs. 5(b) and 5(c). Tunneling events are accelerated by a factor of 2 except for $(U_0, T_0 = -200, 0.0098)$ even in the case with a noticeable difference in $p_{\text{acc}}(\alpha)$ in the high energy region. This implies that the global convergence of simulations of LJ₃₁ is primarily determined by the sampling efficiency around the solid-solid transition region. A modest increase in tunneling events in the case of $(U_0, T_0 = -200, 0.0098)$ is due to sampling performance similar to the t -REM for low temperature replicas as seen in $P_\alpha(U)$ and $p_{\text{acc}}(\alpha)$ in Figs. 3(b) and 5(a), respectively. A strong association between $N_{\tau R}$ and $N_{\tau U}$, i.e., $N_{\tau U}/N_{\tau R} \approx 1$, suggests that more frequent replica exchanges are directly connected to enhanced sampling and more frequent Mackay and anti-Mackay structural transitions.

B. Parametrization schemes II and III

Based on $\tilde{T}_S(U)$ connecting (\tilde{U}_L, T_L) and (\tilde{U}_H, T_H) , we have chosen $\tilde{q}_0 = 0.0075$ in scheme II. Choosing \tilde{q}_0 is a little arbitrary, but the value of \tilde{q}_0 should be smaller than $\tilde{q}_{LH} = (T_H - T_L)/(\tilde{U}_H - \tilde{U}_L) = 0.012$ to avoid multiple crossing points between $\tilde{T}_\alpha^{\text{III}}(U)$ and $T_S(U)$. An alternative choice of \tilde{q}_0 is to set $\tilde{q}_0 = \min\{\tilde{q}_{\alpha\alpha'}\}$ ($\alpha \neq \alpha'$) for all possible combinations of α and α' . We find that the minimum value of $\tilde{q}_{\alpha\alpha'}$ is 0.0086, which is slightly larger than our choice $\tilde{q}_0 = 0.0075$. We also performed the Tsallis-REM simulation with a smaller $\tilde{q}_0 = 0.004$ to investigate the effect of \tilde{q}_0 on the sampling.

In parametrization scheme III, corresponding to Eq. (24), all relevant Tsallis parameters $(\tilde{q}_\alpha, U_\alpha, t_\alpha)$ are determined automatically from the equilibrium phase of a t -REM simulation with predetermined γ . We performed two independent Tsallis-REM simulations with $\gamma = 0.7$ and 0.9 . Compared to the results for scheme I, in Figs. 3(a) and 4(a), the effective temperatures in the Tsallis-REM with $\gamma = 0.9$ shown in Fig. 6(a) are more optimally located to approximate the behavior of $T_S(U)$, with unique stable crossing points at $(\tilde{U}_\alpha, t_\alpha)$.

Due to the concave behavior of $T_S(U)$ between \tilde{U}_1 and \tilde{U}_M , $\tilde{q}_\alpha^{\text{min}} = \tilde{q}_{\alpha M}$ for all replicas corresponding to the slope connecting $(\tilde{U}_\alpha, t_\alpha)$ and (\tilde{U}_M, t_M) . As a result, $\tilde{T}_\alpha(U)$ is almost tangential to $T_S(U)$ with $\tilde{q}_\alpha \approx 0.9T'_S(\tilde{U}_\alpha)$ for higher replicas ($\alpha = 30$ and 35). The resulting Tsallis PDFs in Fig. 6(b) show broader energy distributions even in low temperature regions when compared to the reweighted canonical PDFs,

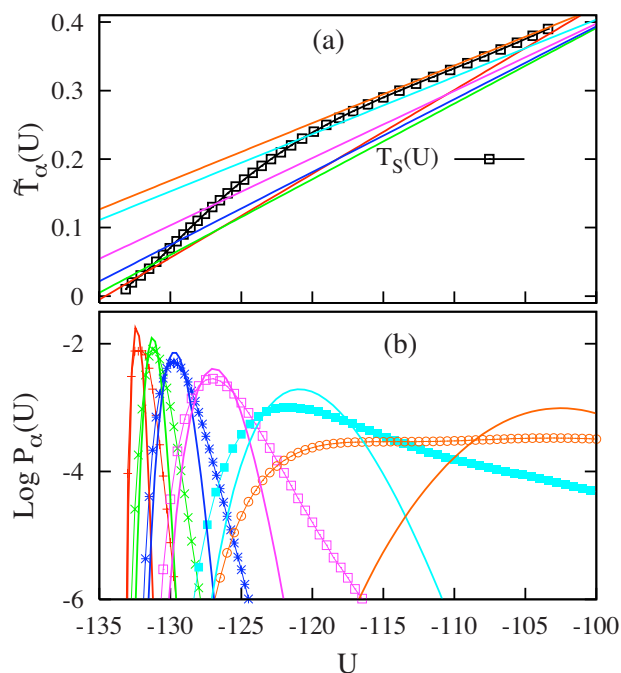


FIG. 6. (Color online) (a) Statistical temperature $T_S(U)$ and Tsallis effective temperatures $\tilde{T}_\alpha^{\text{III}}(U)$ with $\gamma = 0.9$, and (b) Tsallis PDFs (line points) and the reweighted canonical PDFs (solid lines). From bottom to top $\alpha = 10, 15, 20, 25, 30,$ and 35 at $U = -135$ in (a).

and almost uniform energy distributions in $\alpha = 30$ and 35 , in which $\tilde{T}_\alpha^{\text{III}}(U)$ coincides with the linearized $T_S(U)$ at $(\tilde{U}_\alpha, t_\alpha)$.

As seen in Fig. 7(a), the Tsallis-REM provides higher $p_{\text{acc}}(\alpha)$ for all replicas compared to the t -REM even with $\tilde{q}_0 = 0.004$ in scheme II. The enhancement of $p_{\text{acc}}(\alpha)$ is more significant with increasing \tilde{q}_0 and γ in both schemes II and III due to the increased energy overlaps between neighboring replicas. This is a direct result of delocalized Tsallis PDFs. As demonstrated in Figs. 7(b) and 7(c), parametrization scheme III gives the best acceptance of replica exchanges with the most frequent tunneling events in both energy and replica spaces. Compared to the t -REM, the Tsallis-REM with $\gamma = 0.9$ shows 2.5 and 2.2 times more frequent tunneling events in both replica and energy spaces, respectively. The better performance of scheme III can be attributed to the fine tuning of $\tilde{T}_\alpha(U)$ via the optimal determination of \tilde{q}_α , allowing for a more delocalized Tsallis PDF in each replica.

The correlation between tunneling events in replica and energy space, quantified by $N_{\tau R}/N_{\tau U} \approx 1$, falls to 0.9 with increasing γ from 0.7 to 0.9 in scheme III. This implies that a speed up of replica exchanges does not necessarily lead to a direct enhancement of transition between the Mackay global minimum and anti-Mackay isomers, especially for a large energy overlap. This is also observed in the Tsallis-REM employing scheme III with $\gamma = 1$ and $M = 10$, as shown in Fig. 9(b). This is attributed to the combined effects of the enlarged sampling range of each replica and the increased attempt frequency for replica swaps. When replica exchanges are too frequent for a short time period, the swapped configurations are swapped back to the original states before they diffuse or relax to other energy regions.

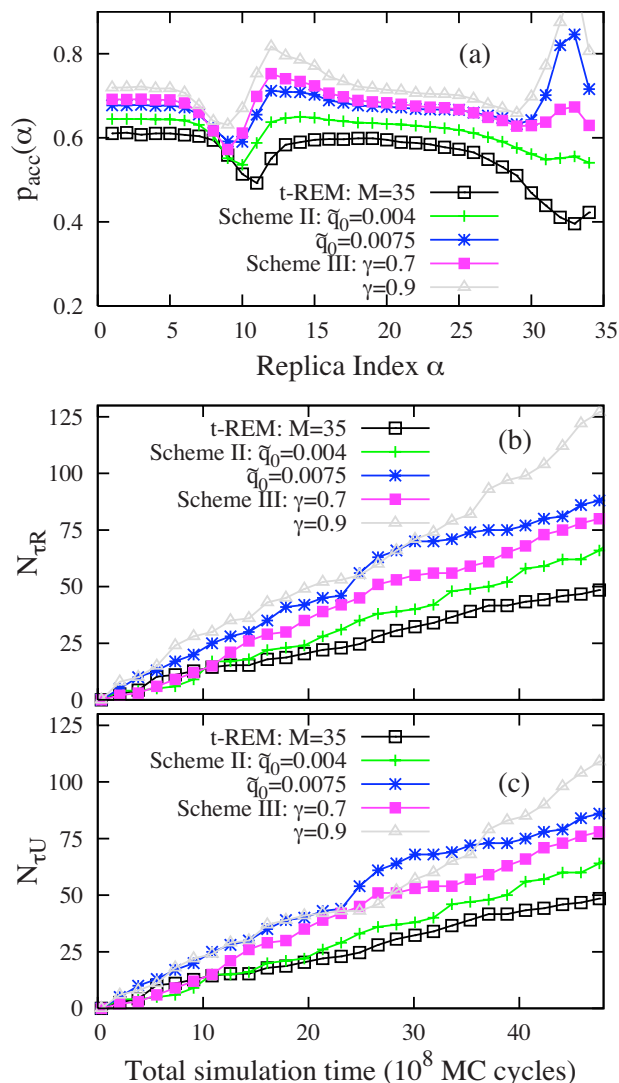


FIG. 7. (Color online) (a) $p_{\text{acc}}(\alpha)$ as a function of the replica index α and accumulated tunneling events in (b) replica space and (c) energy space with varying \tilde{q}_0 in schemes II and γ in scheme III. $N_{\tau U}$ has been determined for the bounded energy region $[-133, -105]$.

C. Tsallis-REM with a smaller M

In comparison to the t -REM, the Tsallis-REM enables more rapid convergence employing the same number of replicas with an enhancement of replica exchanges. This results in the acceleration of tunneling events in both replica and energy space. Our proposed method to determine the optimal Tsallis parameters can be also utilized to mitigate the growth in replica number as \sqrt{f} in the conventional t -REM.

To explore this possibility, we performed three independent Tsallis-REM simulations with a reduced number of replicas such as $M=20$ in scheme II with $\tilde{q}_0=0.0075$, and $M=10$ and 20 in scheme III with $\gamma=1.0$. Note that we used $\gamma=1.0$ in scheme III to maximize energy overlaps and compensate for a smaller M .

As seen in Fig. 8(a), corresponding to scheme III with $M=10$, the Tsallis effective temperatures are optimally aligned to (1) form stable crossing points with $T_S(U)$ for low temperature replicas and (2) locally coincide with $T_S(U)$ at $\tilde{T}_\alpha(U)$ for high temperature replicas. The resulting Tsallis PDFs

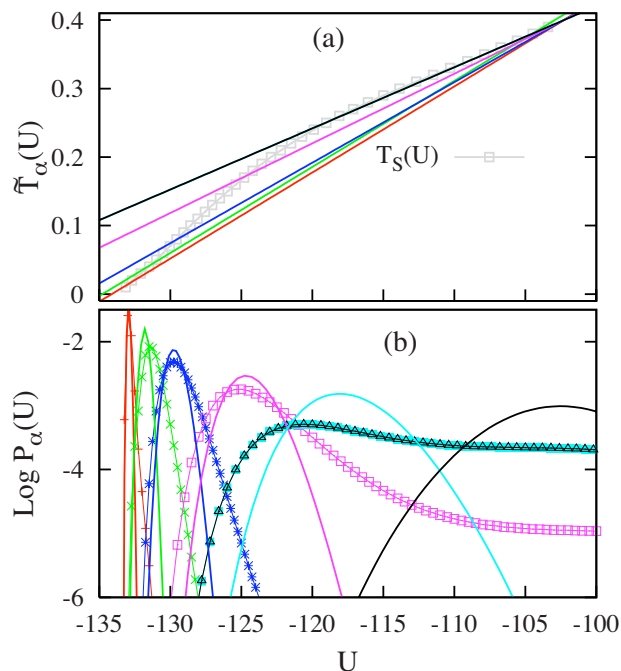


FIG. 8. (Color online) (a) Statistical temperature $T_S(U)$ and Tsallis effective temperatures $\tilde{T}_\alpha(U)$ with $\gamma=1.0$ and $M=10$, and (b) Tsallis PDFs (line points) and the reweighted canonical PDFs (solid lines). From bottom to top $\alpha=2, 4, 6, 8, 9$, and 10 at $U=-135$ in (a). In (a) $\tilde{T}_9(U)$ almost coincides with $\tilde{T}_{10}(U)$, resulting in the superimposed Tsallis PDFs in (b).

in Fig. 8(b) display significant energy overlap between neighboring replicas with delocalized energy distributions, while the overlaps between the reweighted canonical PDFs die away. We find that both $\tilde{T}_9(U)$ and $\tilde{T}_{10}(U)$ have the same $\tilde{q}_\alpha^{\text{min}}=0.09$ due to the concavity in $T_S(U)$. In fact, they are almost superimposed coincidentally as $\tilde{T}_9(U)=0.26+0.09(U+117.4)$ and $\tilde{T}_{10}(U)=0.4+0.09(U+102.3)$. It is remarkable that both $P_9(U)$ and $P_{10}(U)$ are indistinguishable due to the coincidence of $\tilde{T}_9(U)$ and $\tilde{T}_{10}(U)$. This illustrates that $P_\alpha(U)$ is purely determined from the relation between $T_S(U)$ and $\tilde{T}_\alpha(U)$, as in Eq. (13).

The overall acceptance of replica exchanges as a function of t_α in Fig. 9(a) monotonically decays with decreasing M in both schemes II and III except for $\alpha \approx M$. The overall acceptance remains finite for all replicas even with $M=10$ in scheme III, while $p_{\text{acc}}(t_\alpha)$ is essentially zero in the t -REM with $M=10$ (not shown). Due to near perfect energy overlap between $P_9(U)$ and $P_{10}(U)$, replica exchanges between $\alpha=9$ and 10 are always accepted with $p_{\text{acc}}(t_9) \approx 1.0$. This is also seen in scheme III with $M=20$, indicated by $p_{\text{acc}}(t_{20}) \approx 1.0$ in Fig. 9(a). Of particular interest is the acceleration of $N_{\tau R}$ for a smaller M in Fig. 9(b) even with a lower probability of acceptance of replica exchanges. $N_{\tau R}$ in scheme III with $M=10$ and 20 is about two times greater than that of $M=35$, as seen in Fig. 9(b). This trend is also seen in scheme II, where $N_{\tau R}$ is 1.3 times larger in $M=20$ compared to $M=35$.

The enhanced tunneling in replica space with decreasing M results from the combined effects of finite $p_{\text{acc}}(\alpha)$ and increased attempt frequency N_{trial} . Notice that the condition

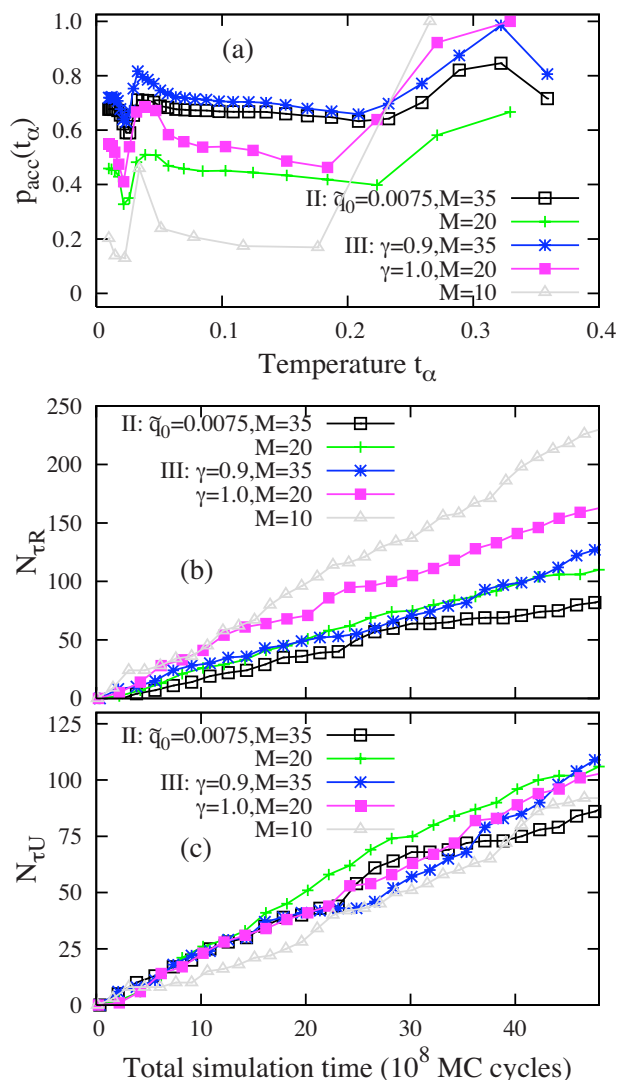


FIG. 9. (Color online) (a) $p_{\text{acc}}(t_\alpha)$ as a function of the temperature t_α and accumulated tunneling events in (b) replica space and (c) energy space with varying a number of replicas (M) in parametrization schemes II and III.

$N_{\text{accept}} = p_{\text{acc}}(\alpha) N_{\text{trial}}$ determines $N_{\tau R}$ for each replica. In the Tsallis-REM, $p_{\text{acc}}(\alpha)$ seems to decrease with M^δ ($\delta < 1$), while N_{trial} increases inversely proportional to M , resulting in $N_{\tau R} \sim M^{(\delta-1)}$. The fit of simulation data with varying M in scheme III gives $\delta \approx 0.5$.

As noted above, the speed up of replica exchanges does not necessarily lead to the acceleration of tunneling events in energy space. In comparison to $N_{\tau U}/N_{\tau R} \approx 1.0$ for $M=35$, smaller ratios $N_{\tau U}/N_{\tau R} \approx 0.38$ and 0.62 are observed in scheme III with $M=10$ and 20 , respectively. This means that recurring replica exchanges for a short time period will not improve the configurational sampling.

In Fig. 10(a), heat capacities of several Tsallis-REM simulations employing different parametrization schemes are compared to those of the t -REM. In both t -REM and Tsallis-REM, an initial simulation of 5×10^8 MC cycles of equilibration was discarded. Heat capacities determined by reweighting for Tsallis-REM simulations for 5×10^9 MC cycles are indistinguishable across the entire temperature region from the reference t -REM data for 10^{10} MC cycles. The robustness of our method is further demonstrated in the mag-

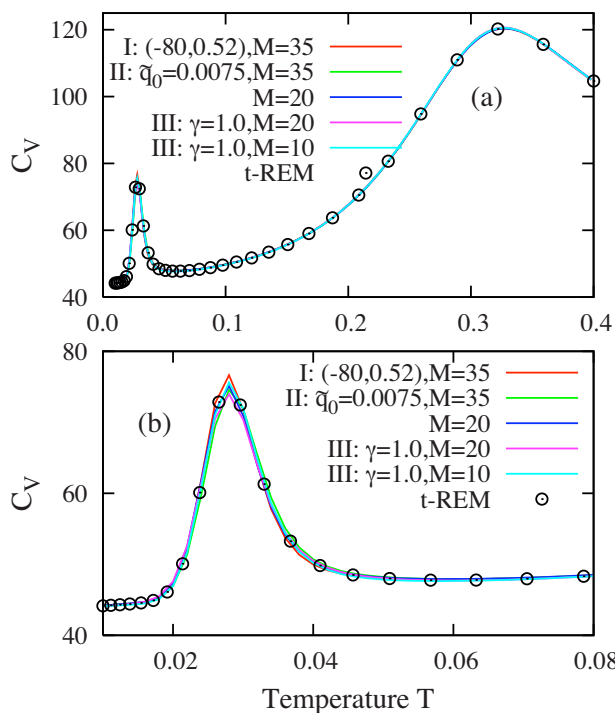


FIG. 10. (Color online) (a) Heat capacities determined by t -REM with $M=35$ for a total 10^{10} MC cycles and Tsallis-REM simulations with different parametrization schemes and M for a total 5×10^9 MC cycles, and (b) magnified view around the Mackay and anti-Mackay transition regions.

nified view of heat capacities at low temperatures in Fig. 10(b). Irrespective of the parametrization scheme and the number of replicas, all Tsallis-REM results show good agreement with the results of the t -REM including a narrow peak in the region corresponding to the solid-solid transition.

V. CONCLUSIONS

In summary, we have developed an effective algorithm for conformational sampling in complex molecular systems through a combination of Tsallis weight sampling and the REM (Tsallis-REM). This method exploits the one-to-one correspondence between the effective temperature and the sampling weight. We presented new parametrization schemes for the Tsallis-REM based on the determination of optimal Tsallis parameters. Compared to the conventional t -REM, our Tsallis-REM enables a considerable enhancement in the acceptance of replica exchanges with optimally chosen Tsallis parameters maximizing the energy overlaps between neighboring replicas.

The accelerated convergence of the Tsallis-REM has been explicitly demonstrated in various simulation conditions of the LJ₃₁ atom cluster by comparing the tunneling events in replica and energy space. The most distinguished feature of our method is that all relevant Tsallis parameters are determined from the equilibrium phase of the conventional t -REM in a fully automated fashion so the method can be straightforwardly implemented into existing replica exchange MC or molecular dynamics simulation codes.

We have also shown that the Tsallis-REM with optimally chosen parameters can significantly reduce the number of replicas without degrading the sampling performance. The

rapid growth in the number of replicas with increased system size is one of the fundamental challenges in the effective application of the conventional t -REM for biomolecules in explicit solvents environments. In most explicit aqueous systems, the statistical temperature monotonically increases as a function of the potential energy due to the dominant energy contribution of the solvent.²⁴ This proposed Tsallis-REM should dramatically improve the system size dependence relative to conventional t -REM through a proper extension to molecular dynamics simulation.

Finally, we would like to emphasize that the effective temperature analysis, applied in this context for the determination of optimal Tsallis parameters, is a general approach that can be applied to the combination of any generalized ensemble sampling and the REM. That can be accomplished by exploiting the one-to-one mapping [Eq. (22)] between the effective temperature and the sampling weight.

ACKNOWLEDGMENTS

We are grateful to the National Science Foundation (Grant No. CHE-0750309) and the National Institutes of Health (Grant No. RO1 GM076688) for the generous support of our research.

- ¹C. J. Geyer and A. Thompson, *J. Am. Stat. Assoc.* **90**, 909 (1995).
- ²K. Hukushima and K. Nemoto, *J. Phys. Soc. Jpn.* **65**, 1604 (1996).
- ³Y. Sugita and Y. Okamoto, *Chem. Phys. Lett.* **314**, 141 (1999).
- ⁴R. Zhou and B. J. Berne, *Proc. Natl. Acad. Sci. U.S.A.* **99**, 12777 (2002).
- ⁵A. E. Garcia and J. N. Onuchic, *Proc. Natl. Acad. Sci. U.S.A.* **100**, 13898 (2003).
- ⁶D. Paschek, S. Gnanakaran, and A. E. Garcia, *Proc. Natl. Acad. Sci. U.S.A.* **102**, 6765 (2005).
- ⁷R. Yamamoto and W. Kob, *Phys. Rev. E* **61**, 5473 (2000).
- ⁸E. Flenner and G. Szamel, *Phys. Rev. E* **73**, 061505 (2006).
- ⁹M. Widom, P. Ganesh, S. Kazimirov, D. Louca, and M. Mihalkovic, *J. Phys.: Condens. Matter* **20**, 114114 (2008).
- ¹⁰H. Liu and K. D. Jordan, *J. Phys. Chem. A* **109**, 5203 (2005).
- ¹¹P. A. Frantsuzov and V. A. Mandelshtam, *Phys. Rev. E* **72**, 037102 (2005); V. A. Mandelshtam and P. A. Frantsuzov, *J. Chem. Phys.* **124**, 204511 (2006).
- ¹²P. Poulain, F. Calvo, R. Antoine, M. Broyer, and Ph. Dugourd, *Phys. Rev. E* **73**, 056704 (2006).
- ¹³B. J. Berne and J. E. Straub, *Curr. Opin. Struct. Biol.* **7**, 181 (1997).
- ¹⁴D. Frenkel and B. Smit, *Understanding Molecular Simulation: From Algorithms to Applications* (Academic, San Diego, 1996).
- ¹⁵M. E. J. Newman and G. T. Barkema, *Monte Carlo Methods in Statistical Physics* (Clarendon, Oxford, 1999).
- ¹⁶H. Fukunishi, O. Watanabe, and S. Takada, *J. Chem. Phys.* **116**, 9058 (2002).
- ¹⁷T. W. Whitfield, L. Bu, and J. E. Straub, *Physica A* **305**, 157 (2002).
- ¹⁸S. Jang, S. Shin, and Y. Park, *Phys. Rev. Lett.* **91**, 058305 (2003).
- ¹⁹P. Liu, B. Kim, R. A. Friesner, and B. J. Berne, *Proc. Natl. Acad. Sci. U.S.A.* **102**, 13749 (2005); P. Liu, X. Huang, R. Zhou, and B. J. Berne, *J. Phys. Chem. B* **110**, 19018 (2006).
- ²⁰X. Cheng, G. Cui, V. Hornak, and C. Simmering, *J. Phys. Chem. B* **109**, 8220 (2005).
- ²¹E. Lyman, F. M. Ytreberg, and D. M. Zuckerman, *Phys. Rev. Lett.* **96**, 028105 (2006).
- ²²S. Trebst, M. Troyer, and U. H. E. Hansmann, *J. Chem. Phys.* **124**, 174903 (2006).
- ²³F. Calvo, *J. Chem. Phys.* **123**, 124106 (2005).
- ²⁴S. W. Rick, *J. Chem. Phys.* **126**, 054102 (2007).
- ²⁵P. Liu and G. A. Voth, *J. Chem. Phys.* **126**, 045106 (2007).
- ²⁶H. Kamberaj and A. van der Vaart, *J. Chem. Phys.* **127**, 234102 (2007).
- ²⁷P. Brenner, C. R. Sweet, D. VonHandorf, and J. A. Izaguirre, *J. Chem. Phys.* **126**, 074103 (2007).
- ²⁸C. Zhang and J. Ma, *Phys. Rev. E* **76**, 036708 (2007).
- ²⁹B. A. Berg and T. Celik, *Phys. Rev. Lett.* **69**, 2292 (1992); *Phys. Lett. B* **267**, 249 (1991).
- ³⁰U. H. E. Hansmann, *Chem. Phys. Lett.* **281**, 140 (1997).
- ³¹U. H. E. Hansmann and Y. Okamoto, *Phys. Rev. E* **56**, 2228 (1997).
- ³²A. Mitsutake, Y. Sugita, and Y. Okamoto, *Biopolymers* **60**, 96 (2001).
- ³³Y. Sugita and Y. Okamoto, *Chem. Phys. Lett.* **329**, 261 (2000).
- ³⁴F. Calvo and J. P. K. Doye, *Phys. Rev. E* **63**, 010902 (2000).
- ³⁵R. Faller, Q. Yan, and J. J. de Pablo, *J. Chem. Phys.* **116**, 5419 (2002).
- ³⁶A. Mitsutake, Y. Sugita, and Y. Okamoto, *J. Chem. Phys.* **118**, 6664 (2003); *J. Chem. Phys.* **118**, 6676 (2003).
- ³⁷C. Tsallis, *J. Stat. Phys.* **52**, 479 (1988).
- ³⁸I. Andricioaei and J. E. Straub, *Phys. Rev. E* **53**, R3055 (1996).
- ³⁹I. Andricioaei and J. E. Straub, *J. Chem. Phys.* **107**, 9117 (1997).
- ⁴⁰Y. Pak and S. Wang, *J. Chem. Phys.* **111**, 4359 (1999).
- ⁴¹I. Fukuda and H. Nakamura, *Phys. Rev. E* **65**, 026105 (2002).
- ⁴²S. Jang, E. Kim, and Y. Pak, *J. Chem. Phys.* **128**, 105102 (2008).
- ⁴³Y. Pak and S. Wang, *J. Phys. Chem. B* **104**, 354 (2000).
- ⁴⁴J. Kim, Y. Fukunishi, and H. Nakamura, *J. Chem. Phys.* **121**, 1626 (2004).
- ⁴⁵J. Kim, Y. Fukunishi, and H. Nakamura, *Phys. Rev. E* **67**, 011105 (2003).
- ⁴⁶J. Kim, Y. Fukunishi, A. Kidera, and H. Nakamura, *Phys. Rev. E* **68**, 021115 (2003).
- ⁴⁷J. Kim, Y. Fukunishi, A. Kidera, and H. Nakamura, *Phys. Rev. E* **69**, 021101 (2004).
- ⁴⁸J. Kim, Y. Fukunishi, A. Kidera, and H. Nakamura, *J. Chem. Phys.* **121**, 5590 (2004).
- ⁴⁹D. A. Kofke, *J. Chem. Phys.* **117**, 6911 (2002); A. Kone and D. A. Kofke, *ibid.* **122**, 206101 (2005).
- ⁵⁰C. Predescu, M. Predescu, and C. V. Ciobanu, *J. Chem. Phys.* **120**, 4119 (2004).
- ⁵¹K. Huang, *Statistical Mechanics* (Wiley, New York, 1972).
- ⁵²A. M. Ferrenberg and R. H. Swendsen, *Phys. Rev. Lett.* **63**, 1195 (1989).
- ⁵³J. Kim, J. E. Straub, and T. Keyes, *Phys. Rev. Lett.* **97**, 050601 (2006); *J. Chem. Phys.* **126**, 135101 (2007); *Phys. Rev. E* **76**, 011913 (2007).
- ⁵⁴J. Kim and T. Keyes, *J. Phys. Chem. B* **112**, 954 (2008).
- ⁵⁵V. A. Sharapov, D. Meluzzi, and V. A. Mandelshtam, *Phys. Rev. Lett.* **98**, 105701 (2007).
- ⁵⁶F. Wang and D. P. Landau, *Phys. Rev. Lett.* **86**, 2050 (2001); F. Wang and D. P. Landau, *Phys. Rev. E* **64**, 056101 (2001).
- ⁵⁷P. Dayal, S. Trebst, S. Wessel, D. Wurtz, M. Troyer, S. Sabhapandit, and S. N. Coppersmith, *Phys. Rev. Lett.* **92**, 097201 (2004).